Global NEST Journal, **28** (XX), pp 1-15
Available online: 16/06/2026

Hydration Mechanism and Microstructure Regulation of CNGA All-Solid-Waste Cementitious Material

Yannian Zhang[a], Qiyue Ren[a], Yingliang Tan[a]*, Qingjie Wang[a], Moncef L. Nehdi[b] and Shunshan Zhang[c]

[a]School of Transportation Engineering, Dalian Jiaotong University, Dalian 116028, China
[b]College of Engineering and Physical Sciences, University of Guelph, Guelph N1G 2W1, Canada
[c]Beijing Building and Apartment Section, China State Railway Beijing Bureau Group Co., Ltd., Beijing 100010, China

*Correspondence e-mail: tanyingliang@djtu.edu.cn

Abstract

To enhance the alkalinity stability of industrial solid wastes during activation, optimize hydration products, and refine microstructure, an all-solid-waste cementitious material (CNGA) was developed in this study. Ground granulated blast furnace slag (GGBS) and bauxite (BA) were used as precursors, while carbide slag (CS) and sodium-based desulfurization ash (NDA) served as dual-alkaline solid waste activators to replace industrial strong alkalis. By systematically adjusting the mix proportion of alkaline solid wastes, NDA dosage, BA dosage, and water-to-binder ratio, the macroscopic mechanical properties were evaluated through compressive strength tests, and the hydration mechanism was investigated using XRD, FTIR, and SEM-EDS. The results indicate that CS–NDA dual-alkaline synergistic activation enables a functional division of rapid alkali elevation and long-term alkali retention, thereby ensuring continuous hydration and suppressing by-product formation. An appropriate NDA dosage significantly enhances the early-age reactivity of GGBS and BA, with an optimal content of 2% achieving a balance between alkaline activation, C–S–H gel formation, and inhibition of side reactions. Furthermore, BA incorporation supplies reactive Al_2O_3, promoting ettringite (AFt) formation and contributing to the generation of C–A–H gel. The SO_4^{2-} in NDA facilitates directional AFt formation, which enhances early-age strength and promotes the development of a gel–crystal composite microstructure.

Keywords: All-solid-waste cementitious materials; Alkali-activated materials; Dual-alkaline solid waste synergistic activation; Gel-crystal composite structure; Hydration products.

Highlights

1. Directionally formed AFt in CNGA interpenetrates C-S-H gel, forming a gel-crystal composite structure as the material's main strength source.
2. CS and NDA achieve alkali source functional division (rapid elevation, long-term retention) through dual-alkaline synergistic activation.
3. The strength contribution of CS manifests in two key aspects: alkaline activation and latent cementitious properties.
4. Optimal NDA dosage balances alkaline activation while inhibiting byproducts (e.g., $CaCO_3$, gypsum).
5. BA contributes by synergistically optimizing the reaction system for an intertwined spatial network, plus supplementary support.

Received: 24/03/2026,

Accepted: 25/05/2026,

Available online: 16/06/2026

Graphical abstract

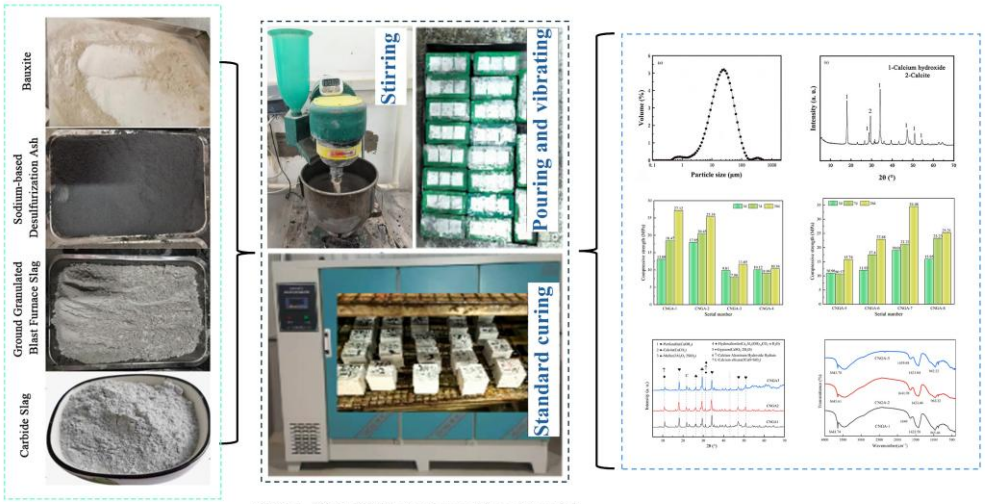

CNGA All-Solid-Waste Cementitious Material

1. Introduction

The cement industry contributes 8–10% of global anthropogenic CO_2 emissions and depends heavily on non-renewable resources such as limestone and clay, posing sustainability challenges (Zhang *et al.* 2025; Kaptan *et al.* 2024; Alsalman *et al.* 2021). In this context, Alkali-Activated Materials have emerged as a promising alternative to Portland cement due to their low carbon footprint and high resource utilization (Kryvenko *et al.* 2024). AAMs based on industrial solid wastes such as GGBS and fly ash enable high-value waste utilization while significantly reducing emissions (Gökçe 2024; Ahmad *et al.* 2024). However, existing studies mainly emphasize basic performance and ngle-system optimization, and from an engineering and high-performance perspective, AAMs still face key bottlenecks in application and performance optimization that limit large-scale use (Sasui *et al.* 2024; Chen and Plank 2024). Firstly, traditional AAMs rely on high-energy, corrosive chemical alkalis such as NaOH and Na_2SiO_3 as activators. This increases production cost and safety risks, and under high alkalinity exacerbates drying shrinkage, induces late-age strength loss, raises chloride penetration risk, and compromises long-term durability. (Quan *et al.* 2025; Dueramae *et al.* 2020). Secondly, chemically synthesized strong alkalis account for 52%–58% of the total cost of conventional two-component AAMs with a 1:2 NaOH–sodium silicate mix. Sodium silicate alone contributes 35%–40% due to its high energy consumption and unit price of about 380 USD per ton, and their combined share exceeds 50%, far higher than that of alkaline solid waste activators (Adesanya *et al.* 2021). Moreover, the high-alkaline environment deteriorates paste fluidity, requiring the additional addition of polycarboxylate superplasticizers to meet construction requirements (Oti *et al.* 2024). Therefore, it is essential to develop alkaline solid waste activation systems without external strong alkalis, to enable low-carbon and large-scale application of AAMs while achieving high-value synergistic utilization of multiple industrial solid wastes.

In recent years, significant progress has been made in solid waste-based alkali-activated systems, with researchers incorporating multiple solid wastes such as carbide slag, sodium-based desulfurization ash, and GGBS into composite cementitious systems. Tripathy *et al.* (2020) found that sodium-based components such as Na^+ increase system alkalinity, accelerate depolymerization of the silico-aluminum network in GGBS, and promote formation of C–(A)–S–H gel, supporting the use of sodium-containing solid wastes such as NDA and soda residue as activation aids. Zheng *et al.* (2024) successfully applied solid sodium silicate to soft soil stabilization, verifying the feasibility of solid alkali activators in engineering practice. Guo *et al.* (2024) further discovered that the synergistic activation of SR and CS can effectively replace strong alkalis such as NaOH, reducing preparation costs; the experiment introduced NDA to rapidly increase initial alkalinity, which significantly promoted early-age hydration reactions. Gu *et al.* (2025) confirmed that the synergy between CS and desulfurization ash effectively supplies Ca^{2+}, OH^-, and SO_4^{2-} to accelerate GGBS hydration, providing valuable insights for solid waste-based activation systems. In addition to studies on alkaline activators, extensive research has also been conducted on the microstructure and hydration products of solid waste-based alkali-activated materials. Marvila *et al.* (2023) systematically investigated the effects of curing regimes and Na_2O concentration on the mechanical properties of alkali-activated cement using ground granulated blast furnace slag as the precursor, and noted that C–S–H gel is the main source of strength development, laying an important foundation for understanding the role of silicate gel in GGBS-based systems. Wang *et al.* (2024) prepared a low-alkali system with a 14-day compressive strength of

45.17 MPa by blending desulfurization gypsum, GGBS, and fly ash; Xu *et al.* (2020) successfully developed clinker-free concrete using SR, GGBS, steel slag, and desulfurization gypsum, achieving a 28-day compressive strength of 38.33 MPa and verifying the feasibility of synergistic utilization of multiple industrial solid wastes. Seo *et al.* (2019) demonstrated that the main hydration products of the CS-ground granulated blast furnace slag binary system are C-A-S-H gel, AFt, and hydrotalcite-like phases, with system strength and pore structure regulated by component ratios. Wang *et al.* (2025) reported that using bauxite tailings and GGBFS as precursors in composite cementitious systems alters the Al/Si ratio, increases hydration product content, and enhances structural complexity and density. These findings provide an important basis for industrial solid waste utilization. However, further analysis indicates that despite progress in single solid waste activation and partial multi-solid waste synergistic activation, significant common bottlenecks remain, as outlined below: (1) Under high sodium-based content conditions, various secondary reactions may occur in the system: for instance, excess SO_4^{2-} may combine with Ca^{2+} to form excessive AFt, leading to volume expansion exceeding the material's bearing capacity and thus damaging the material structure (Yang *et al.* 2024); Na^+ can not only react with CO_2 in the environment to form Na_2CO_3 (Fu *et al.* 2023) but also combine with SO_4^{2-} to generate Na_2SO_4, inducing salt crystallization pressure during wet-dry cycles (Liu *et al.* 2025; Gu *et al.* 2022, 25). Therefore, the optimal dosage range of sodium-based components and their regulatory effect on the composition of hydration products require further clarification. Furthermore, the massive formation of these non-cementitious phases may consume effective calcium sources in the system and affect the pore structure, thereby exerting potential impacts on the formation of C-S-H gel and mechanical properties (Zhu *et al.* 2024; Etcheverry *et al.* 2023). Consequently, the system not only needs a sustained and stable alkaline environment but also requires GGBS, steel slag, and other materials as main silico-aluminum sources to promote the formation of cementitious phases (Zhang *et al.* 2024, 2025). (2) Although solid sodium silicate effectively promotes the initiation of cementitious reactions through an initial high-alkaline environment, its rapid dissolution during hydration may lead to a significant attenuation of system alkalinity over time, making it difficult to maintain a long-term stable high pH environment (Zheng *et al.* 2024). (3) The chemical composition of SR is usually complex, often containing Na_2CO_3 or residual NaOH, and its alkalinity release behavior is greatly influenced by environmental factors (Yang *et al.* 2024; Li *et al.* 2025); meanwhile, the content of reactive aluminum in GGBS and steel slag is relatively limited, which may pose challenges to the precise regulation of the Al/Si ratio and degree of network polymerization in C-(A)-S-H gel (Fu *et al.* 2023; Wang *et al.* 2022). Therefore, introducing aluminum-rich components (e.g., bauxite (BA)) into all-solid-waste cementitious materials and constructing an endogenous, stable alkali activation mechanism may further optimize the hydration product structure and enhance the controllability of material properties (Zheng *et al.* 2024; Wang *et al.* 2022). Li *et al.* (2024) confirmed that the CS–GGBS binary system lacks sulfate and aluminum-rich components, hindering SO_4^{2-}-mediated AFt formation and Al^{3+}-induced cross-linking of the C–S–H network, thus preventing development of a gel–crystal synergistic microstructure. Although these studies provide a foundation for solid-waste utilization, key limitations remain, including unclear regulation of sodium-based components, poor long-term alkalinity stability, and difficulty forming gel–crystal structures due to insufficient aluminum-rich phases, all of which restrict performance optimization and large-scale application. Therefore, expanding component design and introducing multifunctional solid wastes to regulate multiphase hydration products is essential to overcome these challenges.

This study develops a CS–NDA–GGBS–BA CNGA all-solid-waste cementitious material using GGBS and BA as precursors and CS and NDA as activators. Four variable groups including NDA dosage, alkaline solid waste ratio, mineral ratio, and water-to-binder ratio were designed, comprising 18 specimens. Macroscopic properties were evaluated by 3 d, 7 d, and 28 d compressive strength tests, combined with XRD, FTIR, and SEM-EDS analyses. The study systematically reveals the coupled effects of variables on hydration products, microstructure, and mechanical properties, clarifies the self-activation mechanism and microstructure–performance relationship, and provides theoretical and technical support for optimization, engineering application, and low-carbon development of high-performance all-solid-waste cementitious materials.

2. Materials and methods

2.1. *Raw materials and their properties*

In this study, an all-solid-waste cementitious material was prepared with CS and NDA as alkaline solid activators, and GGBS and BA as main precursors. Raw material pretreatment: CS (off-white powder, Yangquan, Shanxi) was dried and ball-milled for 15 min for particle refinement; NDA (coal-fired power plant desulfurization byproduct) was only dried for moisture removal; S105-grade GGBS (Wuhan Iron and Steel Group, GB/T18046) was dried to constant weight at 100±5℃; BA (Hebei metallurgical plant) was dried to constant weight at 100±5℃, ball-milled for activation, and sieved to remove coarse particles.

Prior to testing, all raw materials were dried to below 1% moisture content. CS and BA were further ground at 300 r/min for 15 min to optimize particle size distribution. A laser particle size analyzer (Malvern Mastersizer 2000, UK) and the BET method were then used to measure particle size distribution and specific surface area of the five raw materials, with results presented in **Table 1** and **Figure 1**. Laser particle size analysis showed that the five raw materials had PSDs ranging from 0.1 to 1000 µm, with D50 values of 20.712 µm for CS, 2.255 µm for NDA, 10.568 µm for GGBS, and 43.466 µm for BA. BET results indicated SSAs of 565 m²/kg for CS, 765.69 m²/kg for GGBS, and 447 m²/kg for BA, while NDA exhibited the highest SSA of 2207 m²/kg.

Table 1. Physical properties of CS, NDA, GGBS and BA.

Materials	Particle size parameters			Specific surface area/$m^2 \cdot kg^{-1}$
	D10/μm	D50/μm	D90/μm	
CS	5.945	20.712	59.384	565
NDA	0.318	2.255	12.72	2207
GGBS	2.469	10.568	33.524	765.69
BA	5.487	43.466	104.093	447

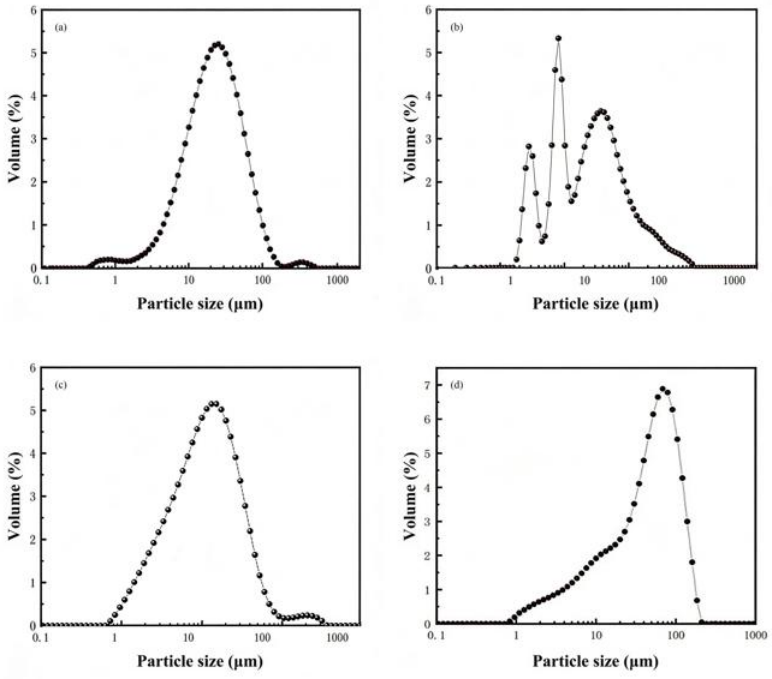

Figure 1. Particle size distribution of (a) CS, (b) NDA, (c) GGBS and (d) BA.

Table 2. Chemical composition and content of CS, NDA, GGBS and BA.

Materials	Mass fraction of each component (%)											
	CaO	SiO_2	Cl	Al_2O_3	MgO	Na_2O	SO_3	Fe_2O_3	TiO_2	MnO	K_2O	P_2O_5
CS	94.737	2.415	-	1.228	-	-	0.779	0.518	0.089	-	-	-
NDA	0.47	0.67	3.30	0.55	0.08	47.91	46.62	0.18	0.05	-	0.07	-
GGBS	49.034	26.641	-	13.123	5.71	0.467	1.933	0.327	1.467	0.687	0.412	-
BA	0.562	21.049	-	69.234	0.181	-	0.092	1.997	6.279	-	0.189	0.218

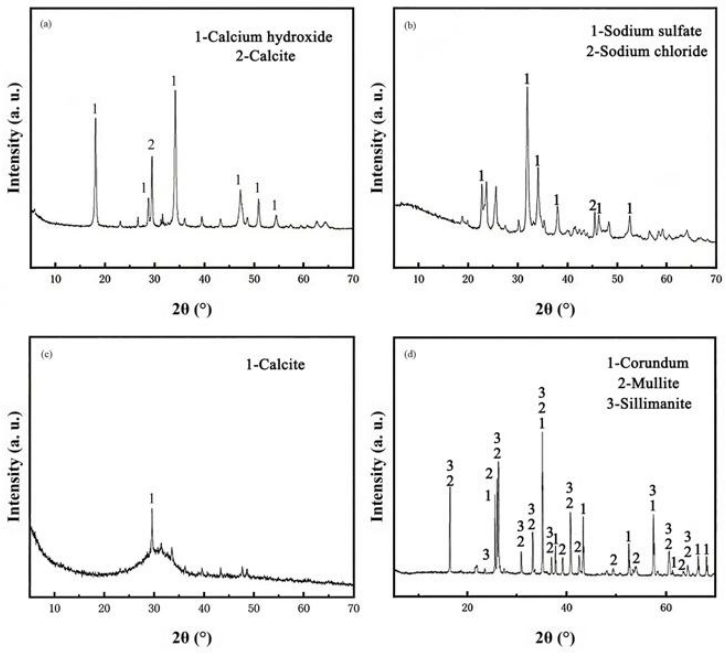

Figure 2. The XRD patterns of raw materials: (a) CS, (b) NDA, (c) GGBS and (d) BA.

X-ray Diffraction (XRD) was used to characterize the chemical composition and mineral phase composition of the five raw materials, with detailed results shown in **Table 2** and **Figure 2**. Analysis showed that CS is dominated by CaO at 94.737%, with calcium hydroxide and calcite as the main phases. NDA mainly contains Na_2O at 47.91% and SO_3 at 46.62%, with sodium sulfate and sodium chloride as primary phases. GGBS is rich in CaO at 49.034% and SiO_2 at 26.641%; its main crystalline phase is calcite, and a broad hump at 20°–40° indicates abundant reactive amorphous aluminosilicates. BA contains high Al_2O_3 at 69.234% and SiO_2 at 21.049%, with corundum, mullite, and sillimanite as major phases. All materials are rich in Ca, Si, and Al, among which Si and Al exhibit pozzolanic reactivity, providing a solid basis for CNGA hydration.

2.2. *Test specimen preparation*

The preparation of paste specimens for the all-solid-waste cementitious material includes three stages: raw material pretreatment, paste preparation, and specimen molding and curing.

(1) Raw material pretreatment: Solid waste materials were dried in an electric thermostatic blast dryer at 105±5℃ for 24 h to ensure moisture content below 1%. The dried materials were mechanically activated using a vertical planetary ball mill (XQM-4), which reduced D50 and enhanced pozzolanic activity.

(2) Paste preparation: Raw materials were weighed according to the designed mix using an electronic balance with 0.01 g accuracy. Mixing water was controlled by pipette based on the preset water-to-binder ratio. A planetary mixer (JJ-5) was used, with 10 s initial mixing, 120 s low-speed mixing, a 15 s rest, and 120 s high-speed mixing to obtain a homogeneous paste.

(3) Specimen molding and curing: 40 mm cube molds were pre-coated with release agent. The paste was placed in three layers and vibrated for 40 s per layer to remove air. After surface leveling, molds were sealed with plastic film and cured at 20±2℃ and relative humidity ≥95% for 24 h. Specimens were then demolded and stored in the curing room under constant conditions until the designated ages.

2.3. *Test methods*

2.3.1. Compressive strength test

Paste specimens in this study were tested with adjusted molding parameters with reference to 'Test Method for Strength of Cement Mortar (ISO Method)'(GB/T17671-2021). Paste samples cured under standard conditions for 3d, 7d, and 28d were subjected to compressive strength testing.

2.3.2. X-ray diffraction (XRD)

The phase composition of raw materials and hydration products was analyzed using a Rigaku D/max-2550 X-ray diffractometer. The operating voltage and current were set to 40 kV and 150 mA, respectively, with Cu Kα radiation as the X-ray source. The scanning range was 5°-70° 2θ at a scanning speed of 5°/min. Jade-6 software was used for the analysis of XRD patterns.

2.3.3. Fourier transform infrared spectroscopy (FTIR)

Fourier transform infrared spectroscopy (FTIR) analysis of hydration product powders was performed using a Nicolet is 10; Nexus 670 spectrometer. The test was conducted in absorbance mode with a wavenumber range of 400–4000 cm^{-1}.

2.3.4. Scanning electron microscopy-energy dispersive spectroscopy (SEM-EDS)

A ZEISS Gemini 300 scanning electron microscope was used to examine the morphology and micro-area composition of hardened paste. Specimens cured to the target age were sampled from the middle, and the fragments were ground and polished into smooth thin sections for analysis of hydration product morphology and composition.

Table 3. CNGA system mix ratio design.

Series	NO.	NDA/%	CS/%	GGBS/%	BA/%	Water-to-binder ratio
Group A: NDA content	CNGA-1	0	40	40	20	0.45
	CNGA-2	2	38	40	20	0.45
	CNGA-3	4	36	40	20	0.45
	CNGA-4	6	34	40	20	0.45
Group B: Alkaline solid waste mix ratio	CNGA-5	0	50	30	20	0.45
	CNGA-6	0	45	35	20	0.45
	CNGA-7	0	35	45	20	0.45
	CNGA-8	0	30	50	20	0.45
Group C: Mineral mix ratio(4%NDA)	CNGA-9	4	36	60	0	0.45
	CNGA-10	4	36	50	10	0.45
	CNGA-3	4	36	40	20	0.45
	CNGA-11	4	36	30	30	0.45
Group C: Mineral mix ratio(0%NDA)	CNGA-12	0	40	60	0	0.45
	CNGA-13	0	40	50	10	0.45
	CNGA-14	0	40	40	20	0.45
	CNGA-15	0	40	30	30	0.45
Group D: Water-to-binder ratio	CNGA-16	4	36	40	20	0.39
	CNGA-17	4	36	40	20	0.42
	CNGA-3	4	36	40	20	0.45
	CNGA-18	4	36	40	20	0.48

Table 4. Effect of different NDA contents on the mechanical properties of the CNGA system.

NO.	NDA Content/%	Compressive strength/MPa		
		3d	7d	28d
CNGA-1	0	13.09	18.47	27.12
CNGA-2	2	17.95	20.45	25.34
CNGA-3	4	9.81	7.86	11.65
CNGA-4	6	10.12	8.99	10.38

2.4. *Experimental scheme*

This study developed an all-solid-waste cementitious material using CS and NDA as alkaline activators and GGBS and BA as precursors. A composite system was designed by varying NDA content, alkaline solid waste proportion, mineral ratio, and water-to-binder ratio. XRD and FTIR were used to identify hydration product types and contents, while SEM-EDS analyzed microstructure and hydration behavior, to clarify the coupled effects of these parameters on material properties and microstructure. The variable levels for each group are detailed in **Table 3**:

3. Results and discussion

3.1. *Macro-performance results and analysis*

3.1.1. Analysis of the effect of NDA content

In this subsection, the NDA content was selected as the primary variable (0%, 2%, 4%, and 6%), with the CS content synchronously adjusted from 40% to 34%. The contents of GGBS (40%) and BA (20%), as well as the water-to-binder ratio (0.45), were kept constant to investigate their effects on the 3-, 7-, and 28-day compressive strengths of the CNGA all-solid-waste cementitious material. The experimental data were presented in **Table 4** and **Figure 3**.

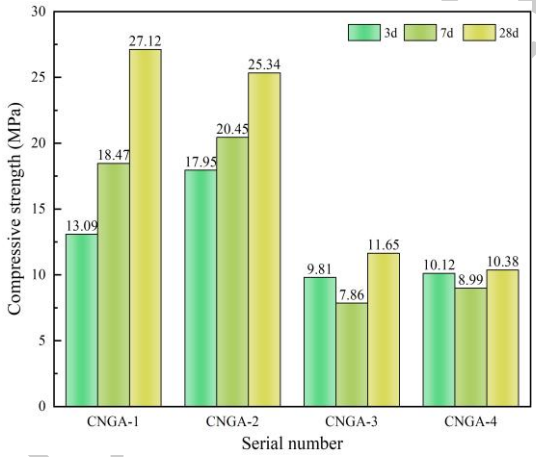

Figure 3 Effect of different NDA contents on the mechanical properties of the CNGA system.

The incorporation of NDA enhanced the early-age reactivity of GGBS and BA. Alkaline components released from NDA accelerated hydration, promoted product formation, and densified the internal structure, improving early-age performance. For CNGA1 with 0% NDA, the 3 d, 7 d, and 28 d compressive strengths were 13.09 MPa, 18.47 MPa, and 27.12 MPa, respectively, showing stable strength development and reflecting the baseline performance without sodium-based activators.

In the CNGA-2 sample containing 2% NDA, the 3d compressive strength increased to 17.95 MPa (a 37% improvement compared to CNGA-1), and the 7d strength reached 20.45 MPa, indicating a significant enhancement in early-age strength. However, the 28d strength slightly decreased to 25.34 MPa. The alkaline components released by the appropriate amount of NDA accelerated the early hydration of GGBS and BA, forming a dense structure. Nevertheless, minor side reactions consumed partial reactive components in the later stage, leading to a slight strength retrogression.

When the NDA content exceeded 2%, the compressive strength of the CNGA system decreased markedly. Excessive NDA induced an over-alkaline environment, which suppressed effective activation of GGBS and BA and reduced the formation of C-S-H gel. Meanwhile, intensified side reactions increased internal porosity and deteriorated matrix compactness, ultimately leading to significant strength loss.

Overall, the CNGA system exhibited optimal compressive strength at an NDA content of 2%, while further increases in NDA dosage led to significant strength reduction due to excessive alkalinity and inhibited hydration.

3.1.2. Analysis of the effect of alkaline solid waste mix ratio

Table 5. Effect of alkaline solid waste mix ratio on compressive strength of CNGA system.

NO.	CS/%	GGBS/%	Compressive strength/MPa		
			3d	7d	28d
CNGA-5	50	30	10.96	10.57	15.74
CNGA-6	45	35	11.93	17.40	22.88
CNGA-7	35	45	19.01	21.21	34.48
CNGA-8	30	50	15.95	23.23	25.21

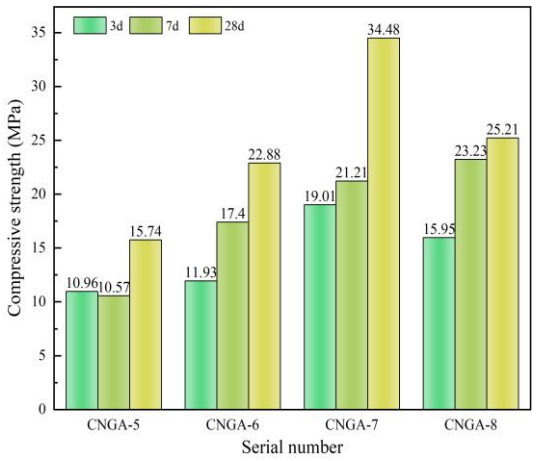

Figure 4. Effect of alkaline solid waste mix ratio on compressive strength of CNGA system.

For this experimental group, the NDA content was fixed at 0%, the BA content at 20%, and the water-to-binder ratio at 0.45. By adjusting the proportion of CS to GGBS (with CS decreasing from 50% to 30% and GGBS increasing synchronously from 30% to 50%), the synergistic effect of alkaline solid wastes and precursors on the strength of the CNGA all-solid-waste cementitious material was investigated. The experimental data were presented in **Table 5** and **Figure 4**.

The compressive strengths of CNGA-5 at 3, 7, and 28 d were 10.96 MPa, 10.57 MPa, and 15.74 MPa, respectively. Its strength was lower than other mixtures: despite sufficient alkalinity from the high CS content, insufficient GGBS limited the supply of reactive components, resulting in inadequate hydration and restrained strength development.

For CNGA-6 (CS reduced to 45%, GGBS increased to 35%), the 3, 7, and 28 d strengths reached 11.93 MPa, 17.40 MPa, and 22.88 MPa, respectively, with a significant strength increase. The results indicate that the higher GGBS proportion facilitated the formation of hydration products and enhanced the material's compactness.

CNGA-7 (CS further reduced to 35%, GGBS increased to 45%) achieved the optimal mechanical properties, with 3, 7, and 28 d strengths of 19.01 MPa, 21.21 MPa, and a peak value of 34.48 MPa, respectively. At this ratio, the alkalinity from CS and reactive components in GGBS reached an optimal balance: sufficient reactive ingredients generated abundant C-S-H gel to fill pores, markedly enhancing matrix density and mechanical strength.

For CNGA-8 (CS decreased to 30%, GGBS increased to 50%), the 3 and 7 d strengths were 15.95 MPa and 23.23 MPa, respectively, but the 28 d strength dropped to 25.21 MPa. Excessively low CS content led to insufficient system alkalinity, causing incomplete GGBS hydration and restricted late-age strength development.

Overall, the CS-to-GGBS ratio exerted a significant influence on the mechanical properties of the CNGA system. The CNGA-7 sample, with 35% CS and 45% GGBS, exhibited the best performance. Excessively high CS content increased porosity and reduced compactness, whereas insufficient CS failed to provide adequate alkalinity to fully activate GGBS, ultimately leading to reduced strength.

3.1.3. Analysis of the effect of BA content

This experimental group investigated the effect of BA content on the compressive strength of CNGA all-solid-waste cementitious material under two scenarios: with and without NDA addition, while analyzed the mechanism of action of BA on the all-solid-waste cementitious material under each scenario. The influence of BA content on the compressive strength of CNGA all-solid-waste cementitious material with NDA addition was presented in **Table 6** and **Figure 5**, while that without NDA addition was shown in **Table 7** and **Figure 6**.

(1) Effect of BA content under 4% NDA addition

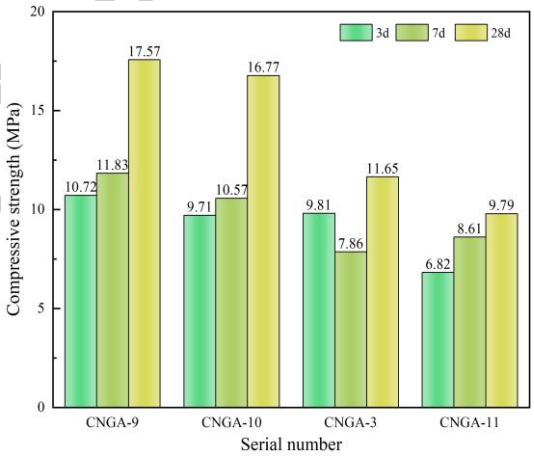

Figure 5. Effect of BA content on compressive strength of CNGA under 4% NDA addition.

For the CNGA-9 sample with 0% BA content, the 3-day, 7-day, and 28-day compressive strengths were 10.72 MPa, 11.83 MPa, and 17.57 MPa, respectively, exhibiting stable strength development. In the absence of BA, the all-solid-waste cementitious material underwent uniform hydration reactions.

With the BA content increased to 10%, the 3d strength slightly decreased to 9.71 MPa, while the 7d and 28d strengths were 10.57 MPa and 16.77 MPa, respectively. These results suggest that a low BA content had no significant influence on the compressive strength of the CNGA system.

Table 6. Effect of BA content on compressive strength of CNGA under 4% NDA addition.

NO.	NDA Content/%	BA Content/%	Compressive strength/MPa		
			3d	7d	28d
CNGA-9	4	0	10.72	11.83	17.57
CNGA-10	4	10	9.71	10.57	16.77
CNGA-3	4	20	9.81	7.86	11.65
CNGA-11	4	30	6.82	8.61	9.79

Elevated BA content significantly degraded the mechanical properties of the CNGA material: 20% BA caused a sharp strength drop (3 d: 9.81 MPa, 7 d: 7.86 MPa, 28 d: 11.65 MPa), which further declined at 30% BA (3 d: 6.82 MPa, 28 d: 9.79 MPa). This stems from uneven reaction between excess BA and NDA, which triggers imbalanced hydration product distribution and higher porosity.

(1) Effect of BA content under 0% NDA addition

Table 7. Effect of BA content on compressive strength of CNGA under 0% NDA addition.

NO.	BA Content/%	Compressive strength/MPa		
		3d	7d	28d
CNGA-12	0	17.09	21.31	47.28
CNGA-13	10	14.93	18.51	33.16
CNGA-14	20	11.53	11.92	26.47
CNGA-15	30	10.24	15.89	19.11

Without NDA addition, the effect of BA content on the compressive strength of the CNGA all-solid-waste cementitious material showed a distinct pattern compared with the 4% NDA group.CNGA-12 (0% BA) achieved the highest overall strength, with 3 d, 7 d, and 28 d compressive strengths of 17.09 MPa, 21.31 MPa, and 47.28 MPa, respectively. This indicates that the CNGA system underwent more complete hydration without NDA and BA, where hydration products filled internal pores to form a denser matrix structure.

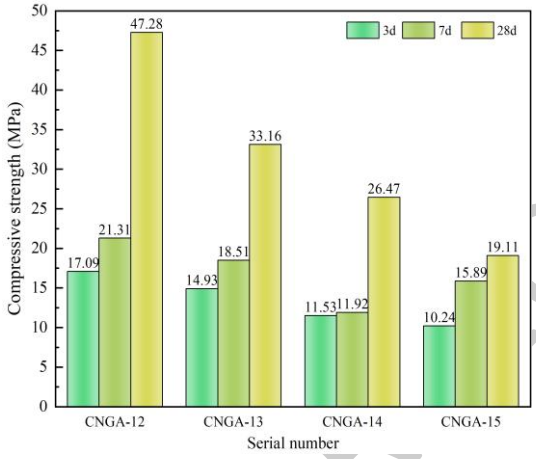

Figure 6. Effect of BA content on compressive strength of CNGA under 0% NDA addition.

Increasing BA content led to continuous strength degradation: 10% BA gave a 3 d strength of 14.93 MPa and 28 d strength of 33.16 MPa (stable but inferior to CNGA-12), which further dropped to 11.53 MPa (3 d) and 26.47 MPa (28 d) at 20% BA, and plummeted to 19.11 MPa at 28 d for 30% BA (a 51% reduction vs. CNGA-12). This severe strength attenuation stems from excessive BA, which cannot participate in effective hydration, increases internal porosity, and inhibits hydration product formation.

Overall, increasing BA content generally exerted a negative effect on the compressive strength of the CNGA system, and this effect was strongly dependent on NDA content. Under 4% NDA addition, excessive BA significantly reduced strength, particularly at BA contents of 20% or higher. In contrast, the system without both BA and NDA achieved the highest strength. These results indicate that BA exhibits relatively low reactivity, and excessive BA primarily increases porosity rather than contributing to effective hydration.

3.1.4. Analysis of the effect of water-to-binder ratio

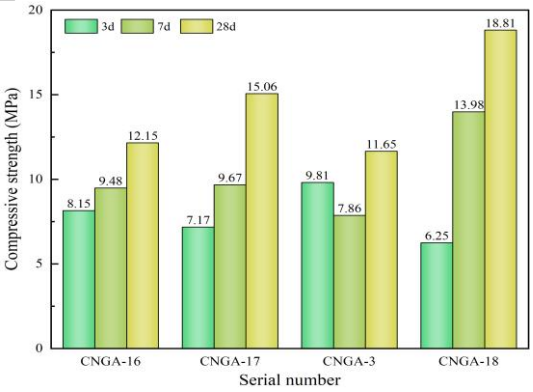

Figure 7. Effect of water-to-binder ratio on the compressive strength of CNGA system.

Table 8. Effect of water-to-binder ratio on compressive strength of CNGA system.

NO.	Water-to-binder ratio	Compressive strength/MPa		
		3d	7d	28d
CNGA-16	0.39	8.15	9.48	12.15
CNGA-17	0.42	7.17	9.67	15.06
CNGA-3	0.45	9.81	7.86	11.65
CNGA-18	0.48	6.25	13.98	18.81

For this experimental group, the NDA content (4%), CS proportion (36%), GGBS proportion (40%), and BA content (20%) were fixed, and a gradient of water-to-binder ratios (0.39, 0.42, 0.45, 0.48) was set for samples CNGA-16 to CNGA-18 and CNGA-3. The aim was to investigate the effect of varying water-to-binder ratios on the compressive strength of CNGA all-solid-waste cementitious material. The influence of the water-to-binder ratio on compressive strength was presented in **Table 8** and **Figure 7**.

For CNGA-16 with a water-to-binder ratio of 0.39, the early-age compressive strengths were relatively high (3 d: 8.15 MPa, 7 d: 9.48 MPa), while the 28 d strength was limited to

12.15 MPa. Although the low water-to-binder ratio reduces free water content and enables the all-solid-waste cementitious material to form a relatively dense structure in the early stage, insufficient moisture restricts late-age hydration reactions. Reactive components such as GGBS and BA cannot be fully dissolved and reacted, resulting in inadequate C-S-H gel formation and slow late-age strength gain.

When the water-to-binder ratio was increased to 0.42 (CNGA-17), the 3d strength decreased to 7.17 MPa (a 12.0% decrease compared to CNGA-16), but the 28d strength increased to 15.06 MPa (a 23.9% increase). A moderate increase in water content improved paste fluidity, facilitating more thorough diffusion of reactants (Ca^{2+}, SiO_2, and Al_2O_3) and more complete late-age hydration. The increased formation of C-S-H gel and AFt offsets the loss of early-age strength.

CNGA3 with a water-to-binder ratio of 0.45 exhibited the lowest strength, with a 28 d compressive strength of 11.65 MPa, 22.6% lower than CNGA17. This ratio led to an imbalance between water and reactive components. Insufficient early hydration limited C–S–H formation and prevented development of a dense microstructure. Although moisture remained at later stages, the lack of early reaction left few reactive components available, restricting formation of sufficient cementitious products for pore filling and resulting in reduced macroscopic strength.

CNGA-18 (water-to-binder ratio 0.48) delivered the group's best long-term mechanical performance, with a 28 d compressive strength of 18.81 MPa (54.8% higher than CNGA-16 at 0.39 water-to-binder ratio). The high water-to-binder ratio sustains late-age hydration: ample moisture enables full dissolution of reactive components in GGBS and BA, forming abundant C-S-H gel and AFt to densify the matrix. Despite a low 3 d strength of 6.25 MPa, the sample achieved significant late-age strength growth.

The water-to-binder ratio had a nonlinear effect on the CNGA system's mechanical properties. The 0.39 ratio benefited early strength but limited late hydration, the 0.48 ratio ensured sufficient moisture for sustained hydration and optimal late-age strength, while the 0.45 ratio performed worst due to water-reactive component imbalance. Thus, 0.48 was identified as the system's optimal water-to-binder ratio.

3.2. *Microscopic analysis of hydration products*

3.2.1. XRD analysis of hydration products

As illustrated in **Figure 8**, multiple reaction products were identified in the CNGA1–3 samples, including calcium silicate hydrate (C–S–H), portlandite ($Ca(OH)_2$), calcite, hydrocalumite, AFt, gypsum, and a small amount of mullite.

NDA enhances the alkaline environment by releasing Na^+. An appropriate dosage promotes GGBS hydration and accelerates C–S–H formation, improving strength. However, excessive NDA creates an overly alkaline environment that suppresses effective C–S–H formation and promotes non-dominant phases such as calcite and hydrocalumite, reducing strength. As the main calcium source, CS supplies Ca^{2+} and OH^- to activate GGBS and BA. Hydration of CaO in CS produces substantial $Ca(OH)_2$, which maintains alkalinity and participates in C–S–H formation.

GGBS is the primary strength contributor in the all-solid-waste cementitious material. Under alkaline conditions, CaO and SiO_2 in GGBS hydrate to form C–S–H gel with an acicular fibrous structure, enhancing matrix compactness and mechanical properties. In CNGA3, this phase evolution aligns with the strength degradation mechanism in Section 3.1.1, where excessive NDA inhibits effective C–S–H formation. By supplying Al_2O_3, BA reacts with Ca^{2+} under alkaline conditions to form hydrocalumite and AFt. An appropriate BA content promotes the formation of C–A–H and hydrocalumite, improving early-age strength and chemical stability.

Table 9. XRD analysis of hydration products in the CNGA system with different sodium-based desulfurization ash contents.

Characteristic peaks (°2θ)	Hydration products	Relationship with performance
18° and 41°	$Ca(OH)_2$	While $Ca(OH)_2$ contributes little directly to strength, the alkaline environment it provides promotes GGBS activation. However, excessive $Ca(OH)_2$ may impair matrix performance by forming calcite through carbonation.
18°,25°and 32°	C-S-H	The higher the C-S-H content, the stronger the matrix cohesion and compactness—making it the primary contributor to the strength of the all-solid-waste cementitious material.
29°and 50°	Calcite	An appropriate amount of Calcite fills internal pores and enhances chemical stability, while excess Calcite increases porosity and weakens mechanical strength.
9.1°,15.7°,18.8°,22.9°and 25.6°	AFt	The formation of AFt contributes to early-age strength development, but excessive AFt may induce expansive cracks in the matrix.
11.6°,20.7°,29.2°and 31.1°	Gypsum	Gypsum is a non-cementitious phase; excessive Gypsum content may lead to increased porosity of the material.
11°and 31°	Hydrocalumite	The flaky structure of Hydrocalumite contributes minimally to strength but enhances the chemical stability of the material.
16°and 33°	Mullite	Mullite exhibits high chemical stability but is a non-cementitious phase, providing limited contribution to the material's strength.

Based on **Table 9** and **Figure 8**, CNGA1 (0% NDA) is dominated by C-S-H (characteristic peaks at 18°, 25°, 32°) and $Ca(OH)_2$ (characteristic peaks at 18°, 41°). A small amount of unreacted phases remains in the system. As the core cementitious phase, C-S-H forms a dense fibrous network, which is consistent with the macroscopic performance of a 28-day compressive strength of 27.12 MPa. $Ca(OH)_2$ provides a stable alkaline environment, with no pronounced carbonation detected.

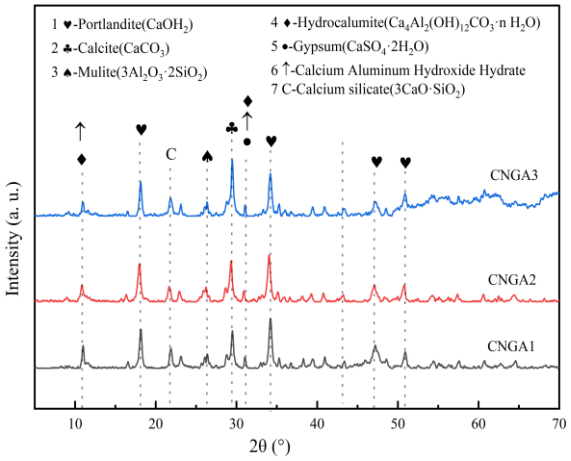

Figure 8. XRD patterns of CNGA1-3 system.

In the CNGA2 (2% NDA) sample, C-S-H and $Ca(OH)_2$ remain the main products, accompanied by a moderate formation of Calcite (characteristic peaks at 29°, 50°), which reflects good compactness. Its 28-day strength (25.34 MPa) is only slightly lower than that of CNGA1.

In CNGA3 with 4% NDA, product composition changes markedly. Calcite and hydrocalumite increase significantly, with characteristic peaks at 11° and 31°, while C–S–H decreases sharply. At the same time, AFt with peaks at 9.1° and 15.7° and gypsum with peaks at 11.6° and 20.7° are enhanced. Non-cementitious phases such as calcite and gypsum become dominant, weakening cohesion and compactness and leading to a sharp reduction in 28 d strength to 11.65 MPa.

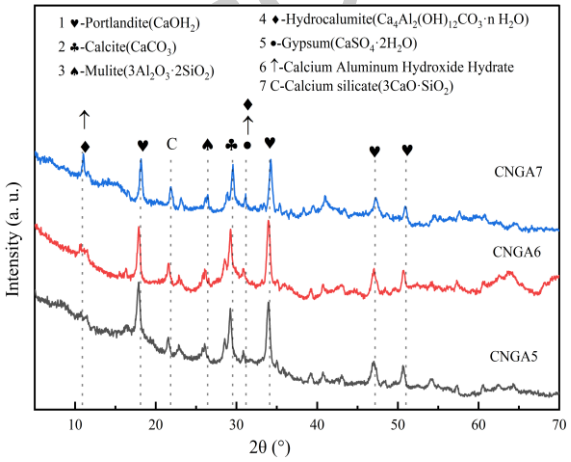

Figure 9. XRD patterns of CNGA5-7 system.

XRD patterns of CNGA5-7 samples are displayed in **Figure 9**. For CNGA5 (50% CS, 30% GGBS), the characteristic peaks of $Ca(OH)_2$ (18°, 41°) are the strongest, while those of C-S-H (18°, 25°, 32°) are relatively weak. As indicated by the intense peaks at 18°, 25°, and 32° in the XRD patterns, although the high $Ca(OH)_2$ content in CNGA5 provides a relatively strong alkaline environment, the insufficient proportion of GGBS restricts the formation of C-S-H. The flaky structure of $Ca(OH)_2$ can offer an alkaline environment for activating GGBS, but it contributes little to strength itself. Additionally, the limited formation of calcite suggests a reduced pore-filling effect, leading to a 28d strength of only 15.74 MPa.

In the CNGA6 sample (45% CS, 35% GGBS), the formation of C-S-H increases, and an appropriate amount of Calcite fills part of the pores. A characteristic peak of Hydrocalumite at 11° emerges, indicating that BA undergoes hydration to form Hydrocalumite under alkaline conditions. Despite its limited contribution to strength, this flaky Hydrocalumite plays a crucial role in enhancing the material's chemical stability. The increased GGBS proportion facilitates the formation of a C-S-H gel network, and Calcite fills partial pores, resulting in an improved 28d strength of 22.88 MPa.

For CNGA7 (35% CS, 45% GGBS), C–S–H formation is maximized, and its fibrous structure forms a dense matrix network. Calcite peak intensity increases, indicating more calcite from $Ca(OH)_2$ carbonation contributes to pore filling. Hydrocalumite and gypsum peaks are also more pronounced, reflecting byproducts of BA reactions under CS activation. These phases assist pore filling and early strength, though excessive amounts may cause microcracking or increased porosity. CNGA7 exhibits the densest microstructure and achieves a 28 d strength of 34.48 MPa, the highest among the three materials.

Overall, C–S–H is the primary cementitious phase controlling CNGA strength. Its formation is enhanced by higher GGBS content and appropriate NDA dosage, improving mechanical performance. $Ca(OH)_2$ mainly provides alkalinity, but excess $Ca(OH)_2$ readily carbonates to calcite, potentially reducing strength. Moderate calcite aids pore filling and stability, whereas excess weakens the matrix. Increasing GGBS is key to strength enhancement, as evidenced by CNGA7 achieving the highest compressive strength.

3.2.2. FTIR analysis of hydration products

FTIR spectra of CNGA1-3 samples are presented in **Figure 10**, and the corresponding absorption peak assignments were summarized in **Table 10**. The absorption peak at 3640 cm^{-1} in the FTIR spectra corresponds to the O-H stretching vibration of $Ca(OH)_2$, originating from the hydration of CaO in CS ($CaO + H_2O \rightarrow Ca(OH)_2$). This peak can be regarded as an indicator of the alkaline environment favorable for C–S–H formation.

CNGA1 shows the strongest $Ca(OH)_2$ absorption peak, indicating higher content that maintains alkalinity for GGBS hydration. With increasing NDA dosage, $Ca(OH)_2$ in CNGA2 and CNGA3 progressively carbonates to calcite, causing a gradual decrease of the 3640 cm^{-1} peak, while calcite peaks at 1420 cm^{-1} and 874 cm^{-1} become more pronounced. In CNGA2, moderate calcite aids pore filling and improves

stability, whereas excessive calcite in CNGA3 increases porosity and reduces mechanical strength.

Absorption peaks at 3400–3200 cm^{-1} and 1600–1680 cm^{-1} correspond to bound water in hydration products, mainly associated with C–S–H gel, and their intensity reflects the degree of hydration. CNGA3 shows relatively strong bound-water peaks under high NDA dosage, indicating an intensified hydration environment. However, the increased bound water did not fully transform into C–S–H; instead, higher amounts of byproducts such as calcite and gypsum adversely affected the strength of the all-solid-waste cementitious material.

Table 10. FTIR absorption peaks for CNGA system.

Wavenumber (cm^{-1})	Corresponding functional groups	Main sources	Relationship with performance
3640	O-H stretching vibration	$Ca(OH)_2$	Provides an alkaline environment, promotes C-S-H formation, and enhances material strength.
1640,3400	H-O-H bending vibration	Bound water in hydration products	Reduced bound water decreases the content of hydration products in the all-solid-waste cementitious material and impairs strength.
1420,874	CO_3^{2-} stretching and bending vibrations	Calcite($CaCO_3$)	As a non-cementitious phase, Calcite inhibits C-S-H formation, increases porosity, and reduces material strength.
960–1000	Si-O-Si stretching vibration	C-S-H, silicates	C-S-H is the primary strength-contributing phase, and a decrease in its content directly impairs the material's performance.
600–700	SO_4^{2-} bending vibration	Gypsum	Gypsum is a byproduct of side reactions that cannot enhance strength and may cause matrix deterioration.

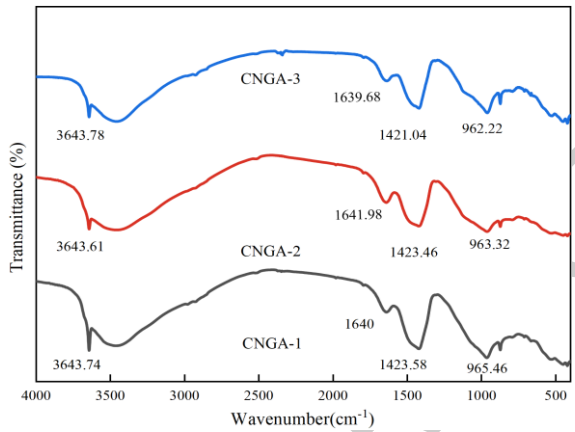

Figure 10. FTIR patterns of sodium group content of CNGA1-3 system.

In the 1100–950 cm^{-1} range, Si–O–Si stretching peaks characteristic of C–S–H indicate the main cementitious phase governing cohesion and compactness. CNGA1 shows the strongest Si–O–Si peak, implying higher C–S–H content and a 28 d strength of 27.12 MPa. CNGA2 has slightly lower C–S–H, but moderate calcite formation aids pore filling, yielding a 28 d strength of 25.34 MPa, close to CNGA1. In CNGA3, C–S–H decreases markedly with the weakest peak intensity; enhanced carbonate- and sulfate-related peaks indicate increased calcite and gypsum, corresponding to reduced C–S–H and weakened mechanical performance.

Gypsum peaks at 600–700 cm^{-1} originate from SO_4^{2-} bending vibrations. CNGA1 contains negligible gypsum. In CNGA2, limited gypsum may aid microstructural densification and early strength. In CNGA3, gypsum increases markedly, likely due to SO_4^{2-} combining with Ca^{2+} at high NDA dosage. As a non-cementitious phase, excess gypsum increases porosity and may reduce long-term strength.

The FTIR spectra of CNGA5–7 samples were shown in **Figure 11**. The O–H stretching peak at ~3640 cm^{-1} corresponds to $Ca(OH)_2$. CNGA5 shows the strongest $Ca(OH)_2$ peak, indicating higher content consistent with its higher CS proportion. While CS supplies abundant Ca^{2+} and OH^-, excess $Ca(OH)_2$ may inhibit effective C–S–H formation. Accordingly, the Si–O–Si band at 1100–950 cm^{-1} (C–S–H) is relatively weak in the FTIR spectra, indicating reduced C–S–H formation and a 28 d compressive strength of 15.74 MPa.

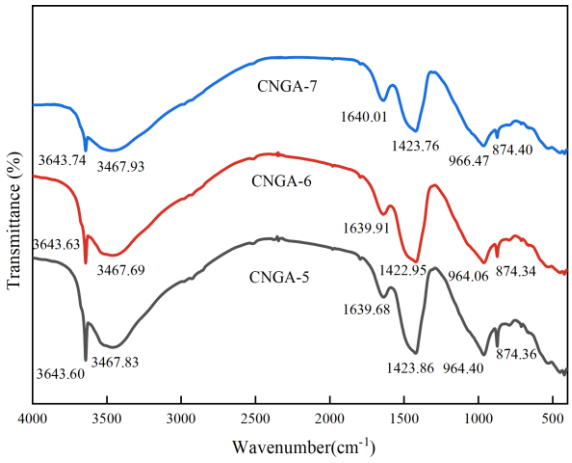

Figure 11. FTIR profile of CNGA5-7 system.

With increasing GGBS content, bound-water bands at 3400–3200 cm^{-1} intensify in CNGA6 and CNGA7, indicating enhanced hydration. Calcite ($CaCO_3$) peaks at ~1410 and 874 cm^{-1} also strengthen, reflecting increased carbonation. In CNGA6, moderate calcite has limited impact on strength, while the enhanced C–S–H peak at 1000–960 cm^{-1} indicates that a 35% GGBS proportion promotes C–S–H gel network formation, yielding a strength of 22.88 MPa.

In CNGA7, where the GGBS proportion is further increased to 45%, the FTIR patterns exhibit the most pronounced

absorption bands associated with Si–O–Si stretching vibration and bound water, indicating a relatively higher degree of C–S–H formation at this ratio. Although the Calcite absorption peak intensifies further (indicating enhanced carbonation), C-S-H remains the dominant phase, forming a dense network structure within the all-solid-waste cementitious material. Consequently, the 28d strength reaches a maximum of 34.48 MPa.

$Ca(OH)_2$ produced by CS hydration provides the alkaline environment required for GGBS activation, but excess $Ca(OH)_2$, as in CNGA5, readily carbonates to calcite. As the primary cementitious phase, C–S–H formation, reflected by the Si–O–Si stretching intensity in FTIR spectra, governs CNGA strength. A moderate amount of calcite, as in CNGA2, can fill micropores, whereas excessive calcite, as in CNGA3, hinders C–S–H interweaving and degrades the microstructure and mechanical properties.

3.2.3. SEM analysis of hydration products

As observed in **Figure 12**, the CNGA1 specimen is relatively dense with low porosity, contributing to improved macroscopic mechanical properties. SEM images show flaky $Ca(OH)_2$ and fibrous C–S–H. $Ca(OH)_2$ presents a regular crystalline morphology and mainly provides an alkaline environment, while fibrous C–S–H forms a continuous network that governs strength. A small amount of unreacted GGBS particles is embedded in the gel matrix with negligible contribution to strength. C–S–H exhibits a typical fibrous or honeycomb-like structure, enhancing matrix bonding. Mineral crystals are tightly bonded without obvious large pores or cracks, indicating a high degree of hydration and uniform reaction in the all-solid-waste cementitious material.

Fibrous C–S–H gel is widely distributed and intertwined to form a dense network, providing the primary strength support for CNGA1, consistent with its 28 d compressive strength of 27.12 MPa. $Ca(OH)_2$ crystals are regular and well dispersed, maintaining a stable alkaline environment that promotes C–S–H formation. A small amount of unhydrated particles is likely due to uneven distribution or locally insufficient alkalinity. Although they have little effect on current strength, they may gradually hydrate at later ages, further enhancing the strength of the all-solid-waste cementitious material.

As illustrated in **Figure 13**, the CNGA3 specimen with 4% NDA and a 28 d compressive strength of 11.65 MPa exhibits obvious cracks and a loose overall structure. Hydration products are scattered and fail to form a dense network. Flaky crystals, presumed to be hydrocalumite, show high chemical stability but a loose structure with limited contribution to strength. Unlike the fibrous C–S–H network in CNGA1, no distinct C–S–H network is observed in CNGA3, indicating that excessive NDA may inhibit its formation. Numerous uniformly distributed granular particles are identified as calcite $CaCO_3$, likely formed by early carbonation under high NDA content. No evident binding phase or dense filling is observed between particles, reflecting weak bonding performance.

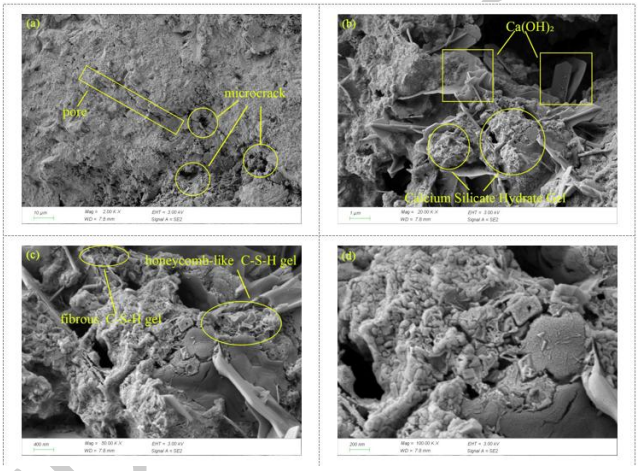

Figure 12. Scanning electron micrograph of CNGA1 specimen 28d.

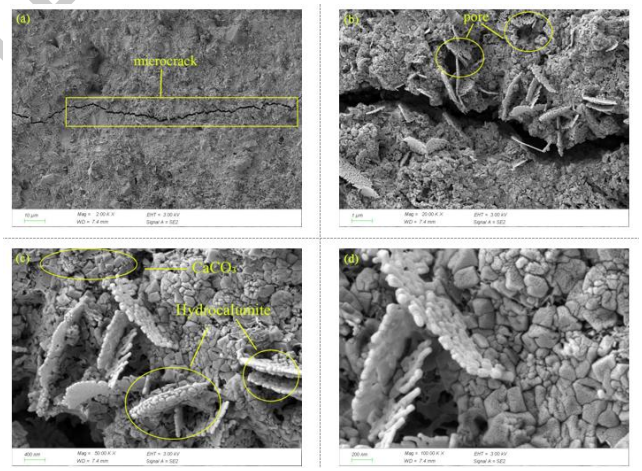

Figure 13. Scanning electron micrograph of CNGA3 specimen 28d.

Table 11. Comparison of CNGA1 and CNGA3 systems.

Characteristics	CNGA1	CNGA3
Porosity	Low	High
Hydration Products	Dominated by C-S-H, with $Ca(OH)_2$ as the secondary phase	Dominated by Calcite ($CaCO_3$) and Hydrocalumite
Microstructure	Dense	Loose with numerous cracks
28-day Compressive Strength	27.12MPa	11.65MPa

At high NDA dosage, substantial $CaCO_3$ forms from the carbonation of $Ca(OH)_2$. Although chemically stable, $CaCO_3$ contributes little to strength and hinders C–S–H formation. Elevated NDA enhances Al_2O_3 reactivity, promoting hydrocalumite formation, but its loose flaky structure offers limited strength gain. Extensive cracks and pores are consistent with the low 28 d compressive strength of 11.65 MPa. The high porosity and loose structure markedly

reduce CNGA3 strength. SEM shows a loose matrix with abundant granular calcite and flaky hydrocalumite, while a continuous C–S–H network is absent, accounting for the low compressive strength. A comparison between CNGA1 and CNGA3 is provided in **Table 11**.

4. Conclusions

Through systematic macroscopic and microscopic analyses, this study investigates the hydration characteristics and reaction mechanisms of all-solid-waste cementitious materials prepared by activating a GGBS–BA precursor with a CS–NDA composite alkaline activator. Four key factors, namely alkaline solid waste ratio, NDA dosage, water-to-binder ratio, and precursor proportion, were evaluated for their effects on workability, mechanical properties, and microstructural evolution using XRD, FTIR, and SEM-EDS. The main conclusions are as follows:

1. In CNGA all-solid-waste cementitious materials, SO_4^{2-} reacts with C–A–H gel from GGBS hydration and Ca^{2+} supplied by CS to preferentially form AFt. This AFt, with acicular or columnar morphology, interpenetrates the C–S–H gel framework, enhancing mechanical interlocking and filling micropores between gel particles. Together, these effects create a gel–crystal composite structure that serves as the primary source of strength.
2. The high-alkaline environment established by CN dual-alkaline synergistic activation enables a functional division of alkali sources, featuring rapid alkalinity increase and sustained retention. An appropriate NDA dosage provides highly active alkali, and the high solubility of Na^+ quickly raises the pH of the system. Meanwhile, CS acts as a stable alkali reservoir, where $Ca(OH)_2$ gradually dissolves to maintain long-term alkalinity and prevent sudden pH decline. As a result, CN dual-alkaline activation overcomes the limitations of slow alkali development and unstable alkalinity in single solid-waste systems.
3. CS contributes to strength development in CNGA all-solid-waste cementitious materials through both alkaline activation and latent cementitious properties. It supplies OH^- to create a high-alkaline environment, breaking down inert layers on GGBS and BA and promoting formation of C–S–H and AFt. It also provides abundant Ca^{2+}, which reacts with SiO_3^{2-} and AlO_2^- to form C–(A)–S–H gel. In sulfate-containing systems, CS further reacts with sulfates to generate limited AFt, aiding pore filling and microstructural densification.
4. NDA dosage significantly affects strength, with an optimal level of 2% balancing alkaline activation and suppression of side reactions. This dosage enhances the hydration of GGBS and BA, promotes C–S–H formation, and produces a small amount of $CaCO_3$ for pore filling, thereby improving strength. Excessive NDA is unfavorable, as non-cementitious byproducts become dominant and hinder strength development.
5. CS provides the activation environment, NDA stabilizes it and regulates product types, GGBS supplies the main cementitious products, and BA contributes reactive components to enhance chemical stability. Together, the CNGA system forms an integrated control framework covering effective activation, stable reactions, cementitious product formation, and dense structural development.

CRediT authorship contribution statement

Qiyue Ren: Data curation, Formal analysis, Investigation, Methodology, Visualization, Writing-original draft. Yannian Zhang: Data curation, Formal analysis, Investigation, Methodology, Visualization, Writing-original draft, Project administration, Funding acquisition. Yingliang Tan: Project administration, Supervision, Writing-original draft, Funding acquisition. Qingjie Wang: Investigation, Supervision, Writing - review & editing. Moncef L. Nehdi: Investigation, Supervision, Writing - review & editing. Shunshan Zhang: Investigation, Supervision, Writing - review & editing.

LLM Usage Declaration

During the preparation of this manuscript, we used ChatGPT (OpenAI) solely for language polishing and grammatical correction of the full text, to improve the readability and fluency of the English expression. The tool was not used to generate any research content, design experiments, process or analyze experimental data, or interpret research results. All scientific concepts, experimental designs, data analysis, research conclusions and core content of this manuscript are the original work of the authors.

Declaration of Competing Interest

The authors declare that they have no known competing financial interests or personal relationships that could have appeared to influence the work reported in this paper.

Acknowledgments

Funding: This work was supported by the Key Project of National Natural Science Foundation of China (No. 52234004), the Key Research and Development Project of the Science and Technology Plan of Liaoning Province-Industrial Technology Innovation Category (No. 2024JH2/102400016), the Basic Research Project of the Department of Education of Liaoning Province (LJ212510150005), and the Science and Technology Plan Project of the Department of Housing and Urban-Rural Development of Liaoning Province (LNSJSKJ-2025-060).

References

Adesanya E., P. Perumal, T. Luukkonen, J. Yliniemi, K. Ohenoja, P. Kinnunen, M. Illikainen, Opportunities to improve sustainability of alkali-activated materials: A review of side-stream based activators, Journal of Cleaner Production 286 (2021).http://dx.doi.org/10.1016/j.jclepro.2020.125558

Ahmad M.R., A. Fernàndez-Jimenez, B. Chen, Z. Leng, J.-G. Dai, Low-carbon cementitious materials: Scale-up potential, environmental impact and barriers, Construction and Building Materials 455 (2024).http://dx.doi.org/10.1016/j.conbuildmat.2024.139087

Alsalman A., L.N. Assi, R.S. Kareem, K. Carter, P. Ziehl, Energy and CO_2 emission assessments of alkali-activated concrete and

ordinary portland cement concrete: A comparative analysis of different grades of concrete, Cleaner Environmental Systems 3 (2021).http://dx.doi.org/10.1016/j.cesys.2021.100047

Chen J., J. Plank, Alkali-activated calcined clay blended cement: Effect of NaOH activator on performance of HPEG PCEs and on early strength, Cement and Concrete Research 183 (2024) 14.http://dx.doi.org/10.1016/j.cemconres.2024.107588

Dueramae S., W. Tangchirapat, P. Chindaprasirt, C. Jaturapitakkul, P. Sukontasukkul, Autogenous and drying shrinkages of mortars and pore structure of pastes made with activated binder of calcium carbide residue and fly ash, Construction and Building Materials 230 (2020) 9.http://dx.doi.org/10.1016/j.conbuildmat.2019.116962

Etcheverry J.M., Y.A. Villagran-Zaccardi, P. Van den Heede, V. Hallet, N. De Belie, Effect of sodium sulfate activation on the early age behaviour and microstructure development of hybrid cementitious systems containing portland cement, and blast furnace slag, Cement and Concrete Composites 141 (2023).http://dx.doi.org/10.1016/j.cemconcomp.2023.105101

Fu Q., M. Bu, Z. Zhang, W. Xu, Q. Yuan, D. Niu, Hydration characteristics and microstructure of alkali-activated slag concrete: A review, Engineering 20 (2023) 162–179.http://dx.doi.org/10.1016/j.eng.2021.07.026

GB/T 17671-2021, Method of testing cements-determination of strength (ISO method).2021

Gökçe H.S., Durability of slag-based alkali-activated materials: A critical review, Journal of the Australian Ceramic Society 60(3) (2024) 885–903.http://dx.doi.org/10.1007/s41779-024-01011-z

Gu X., X. Li, Y. Zhao, J. Liu, Z. Hu, Z. Hu, Effect of desulfurization ash and carbide slag double-mixture on hydration of slag-based cementitious materials, Metal Mine (02) (2025) 240–246.http://dx.doi.org/10.19614/j.cnki.jsks.202502032

Gu Y., P. Dangla, R.-P. Martin, o. metalssi-omikrine, T. Fen-Chong, Modeling the sulfate attack induced expansion of cementitious materials based on interface-controlled crystal growth mechanisms, Cement and Concrete Research 152 (2022) 15.http://dx.doi.org/10.1016/j.cemconres.2021.106676

Guo W., Q. Zhao, Y. Qiu, Y. Shi, S. Wang, Basic mechanical properties and stress-strain relationship of soda residue-calcium carbide slag activated concrete, Materials Reports 38(17) (2024) 140–147.http://dx.doi.org/10.11896/cldb.22070247

Ji X, Z. Wang, X. Wang, X. Zhao, H. Zhang, T. Zhang, Microstructures and properties of alkali-activated slags with composite activator: Effects of Na2O equivalents, Journal of Cleaner Production 450 (2024).http://dx.doi.org/10.1016/j.jclepro.2024.141754

Kaptan K., S. Cunha, J. Aguiar, A review: Construction and demolition waste as a novel source for CO2 reduction in portland cement production for concrete , Sustainability 16(2) (2024).http://dx.doi.org/10.3390/su16020585

Kryvenko P., I. Rudenko, P. Sikora, M. Sanytsky, O. Konstantynovskyi, T. Kropyvnytska, Alkali-activated cements as sustainable materials for repairing building construction: A review, Journal of Building Engineering 90 (2024) 27.http://dx.doi.org/10.1016/j.jobe.2024.109399

Li Y., S. Duan, H. Wu, X. Shi, X. Han, P. Zhao, Z. Ma, Mechanical properties and hydration mechanism of red mud-fly ash-calcium carbide slag composite cementitious materials, Bulletin of the Chinese Ceramic Society 44(03) (2025) 1041–1049.http://dx.doi.org/10.16552/j.cnki.issn1001-1625.2024.1104

Li Z., K. Xu, N. Sun, J. Wang, K. Xue, L. Xu, Y. Ren, Z. Yan, T. Sima, Compressive strength and microstructure of carbide slag and alkali-activated blast furnace slag pastes in china, Buildings 14(6) (2024).http://dx.doi.org/10.3390/buildings14061681

Liu L., X. Chen, K. Pang, A. Neupane, L. Xie, D. Shen, Degradation of alkali-activated slag pastes exposed to high-concentration chloride, sulfate and magnesium multi-salt solutions, Construction and Building Materials 464 (2025) 15.http://dx.doi.org/10.1016/j.conbuildmat.2025.140182

Marvila M.T., A.R. Garcez de Azevedo, J.A. Tostes Linhares Júnior, C.M. Fontes Vieira, Activated alkali cement based on blast furnace slag: Effect of curing type and concentration of Na2O, Journal of Materials Research and Technology 23 (2023) 4551–4565.http://dx.doi.org/10.1016/j.jmrt.2023.02.088

Oti J., B.O. Adeleke, F.X. Anowie, J.M. Kinuthia, E. Ekwulo, Mechanical properties of a sustainable low-carbon geopolymer concrete using a pumice-derived sodium silicate solution, Materials 17(8) (2024) 16.http://dx.doi.org/10.3390/ma17081792

Quan, G. Zhao, X. Liu, M. Bu, Investigation on the sodium silicate modulus-affected macroscopic and microscopic characteristics of alkali-activated slag concrete, Materials Science and Technology (2025) 14.http://dx.doi.org/10.1177/02670836241306659

Sasui S., G. Kim, A. van Riessen, H. Eu, J. Park, J. Nam, C. Lim, Effects of Na2SiO3/NaOH ratio in alkali activator on the microstructure, strength and chloride ingress in fly ash and GGBS based alkali activated concrete, Journal of Building Engineering 98 (2024) 17.http://dx.doi.org/10.1016/j.jobe.2024.111255

Seo J., S. Park, H.N. Yoon, J.G. Jang, S.H. Kim, H.K. Lee, Utilization of calcium carbide residue using granulated blast furnace slag, Materials 12(21) (2019).http://dx.doi.org/10.3390/ma12213511

Tripathy S.K., J. Dasu, Y.R. Murthy, G. Kapure, A.R. Pal, L.O. Filippov, Utilisation perspective on water quenched and air-cooled blast furnace slags, Journal of Cleaner Production 262 (2020).http://dx.doi.org/10.1016/j.jclepro.2020.121354

Wang H., X. Zhao, T. Wang, L. Su, B. Zhou, Y. Lin, Determination of gel products in alkali-activated fly ash-based composites incorporating inorganic calcium additives, Advances in Materials Science and Engineering 2022 (2022) 1–13.http://dx.doi.org/10.1155/2022/7476671

Wang L., H. Chen, Y. Zhang, Study on mechanical properties and hydration characteristics of bauxite-GGBFS alkali-activated materials, based on composite alkali activator and response surface method, Materials 18(7) (2025).http://dx.doi.org/10.3390/ma18071466

Xu D., W. Ni, Q. Wang, C. Xu, Y. Jiang, Preparation of clinker-free concrete by using soda residue composite cementitious material, Journal of Harbin Institute of Technology 52(08) (2020) 151–160.http://dx.doi.org/10.11918/201909069

Yang G., C. Li, W. Xie, Y. Yue, C. Kong, X. Li, Effect of carbide slag and steel slag as alkali activators on the key properties of carbide slag-steel slag-slag-phosphogypsum composite cementitious materials, Frontiers in Materials 11 (2024).http://dx.doi.org/10.3389/fmats.2024.1353004

Zhang L., Y. Zhang, Q. Wang, W. Zhang, Z. Li, Y. Shang, H.-Q. Sun, Effects of two activators on the hydration characteristics and microstructure of lithium slag-steel slag-containing composite cementitious materials, Construction and Building Materials 483 (2025). http://dx.doi.org/10.1016/j.conbuildmat.2025.141749

Zhang S., Y. Zhang, J. Zhang, Y. Li, Compressive strength and resistance to sulphate attack of ground granulated blast furnace slag, lithium slag, and steel slag alkali-activated materials, Buildings 14(8) (2024).http://dx.doi.org/10.3390/buildings14082320

Zhang Y., W. Liu, Q. Wang, L. Zhang, Coupling mechanisms and synergistic effects in portland cement-ceramic powder-ground granulated blast furnace slag-CFB desulfurization ash compositebinder , Waste and Biomass Valorization (2025).http://dx.doi.org/10.1007/s12649-025-03270-8

Zheng Y., J. Wu, A. Yang, B. Li, L. Gu, Feasibility study on the one-part geopolymer activated by solid sodium silicate for soft soil solidification, Rock and Soil Mechanics 45(07) (2024) 2072–2084.http://dx.doi.org/10.16285/j.rsm.2023.1290

Zhu J., H. Cui, L. Cui, S. Yang, C. Zhang, W. Liu, D. Zheng, Mutual activation mechanism of cement-GGBS-steel slag ternary system excited by sodium sulfate, Buildings 14(3) (2024) 17.http://dx.doi.org/10.3390/buildings14030631